

Broad Learning System Based on Maximum Correntropy Criterion

Yunfei Zheng, Badong Chen, *Senior Member, IEEE*, Shiyuan Wang, *Senior Member, IEEE*, and Weiqun Wang, *Member, IEEE*

Abstract—As an effective and efficient discriminative learning method, Broad Learning System (BLS) has received increasing attention due to its outstanding performance in various regression and classification problems. However, the standard BLS is derived under the minimum mean square error (MMSE) criterion, which is, of course, not always a good choice due to its sensitivity to outliers. To enhance the robustness of BLS, we propose in this work to adopt the maximum correntropy criterion (MCC) to train the output weights, obtaining a correntropy based broad learning system (C-BLS). Thanks to the inherent superiorities of MCC, the proposed C-BLS is expected to achieve excellent robustness to outliers while maintaining the original performance of the standard BLS in Gaussian or noise-free environment. In addition, three alternative incremental learning algorithms, derived from a weighted regularized least-squares solution rather than pseudoinverse formula, for C-BLS are developed. With the incremental learning algorithms, the system can be updated quickly without the entire retraining process from the beginning, when some new samples arrive or the network deems to be expanded. Experiments on various regression and classification datasets are reported to demonstrate the desirable performance of the new methods.

Index Terms—Broad Learning System, maximum correntropy criterion, incremental learning algorithms, regression and classification.

I. INTRODUCTION

Broad Learning System (BLS) [1] is an emerging discriminative learning method, which has been shown with the potential to outperform some deep neural network based learning methods, such as multilayer perceptron-based methods (MLP) [2], deep belief networks (DBN) [3], and stacked auto encoders (SAE) [4]. To design a BLS, there are several necessary steps, including: 1) transforming the input data into general mapped features by some feature mappings; 2) the generated mapping features are connected by nonlinear activation functions to form the so called the “enhancement nodes”; 3) the mapped features and the “enhancement nodes” are sent together into the output layer, and the corresponding

output weights are obtained by the means of pseudo-inverse. Since all weights and biases of the hidden layer units in BLS can be randomly generated and remain unchanged after that, we only need to train the weights between the hidden layer and the output layer, which brings great convenience to the training process. In addition, if some new samples arrive or the network deems to be expanded, several practical incremental learning algorithms were developed to guarantee that the system can be remodeled quickly without the entire retraining process from the beginning [1]. Thanks to these attractive features, BLS has received increasing attention [5]–[17] and been successfully applied in image recognition, face recognition, time series prediction, etc.

The standard BLS, however, takes the minimum mean square error (MMSE) criterion as a default choice of the optimization criterion in training the network output weights. Although MMSE criterion is computationally efficient and can provide good performance in Gaussian or noise-free environments, it will degrade the performance of BLS in complicated noise environments especially when data are contaminated by some outliers. To address this issue, several alternative optimization criteria which combine l_1 -norm with different regularization terms were proposed to train the output weights of BLS, generating a class of robust BLS (RBLS) variants [9]. Since l_1 -norm is less sensitive to outliers, the robustness of BLS has been significantly improved. Along the same line, Chu et al. [18] put forward the weighted BLS (WBLS). With the well-designed weighted penalty factor, WBLS has shown good robustness in nonlinear industrial process. Another representative work to improve the robustness of BLS is the robust manifold BLS (RM-BLS) [19]. By introducing the manifold embedding and random perturbation approximation, the robust mapping features can be expected in some special application scenarios, like the noisy chaotic time series prediction. Therefore, RM-BLS also has the ability to improve the robustness of BLS.

Although the aforementioned robust BLS variants can be good candidates when some training data are disturbed by outliers, they suffer from some drawbacks. For example, due to computational complexity, the incremental learning algorithms have not been provided under l_1 -norm based optimization criteria, even though they are one of the most important features of the standard BLS. For WBLS, its performance depends on the weighted penalty factor which needs to be specified in advance. In addition, the abandonment of the connections between the input layer and the feature layer may lose some interesting proprieties [1], [5]–[7], [10], and even

Yunfei Zheng and Badong Chen (corresponding author) are with the Institute of Artificial Intelligence and Robotics, Xi’an Jiaotong University, Xi’an 710049, China (e-mail: zhengyf@stu.xjtu.edu.cn; chenbd@mail.xjtu.edu.cn).

Shiyuan Wang is with the College of Electronic and Information Engineering, Southwest University, Chongqing 400715, China (e-mail: wsy@swu.edu.cn).

Weiqun Wang is with the State Key Laboratory of Management and Control for Complex Systems, Institute of Automation, Chinese Academy of Sciences, Beijing 100190, China (e-mail: weiqun.wang@ia.ac.cn).

This work was supported by National Natural Science Foundation of China (91648208, 61976175), National Natural Science Foundation-Shenzhen Joint Research Program (U1613219), and The Key Project of Natural Science Basic Research Plan in Shaanxi Province of China (2019JZ-05).

makes WBLs fall into some common pitfalls discussed in [20]. As for RM-BLS, the random perturbation matrix is of great importance to promote the robustness of the algorithm, but how to design such random perturbation matrix is lack of guidance at present. Therefore, to develop a more general BLS which is expected to remain the advantages of the standard BLS as possible while having the ability to suppress the adverse effects of outliers still needs more efforts.

During the past few years, an efficient Information Theoretic Learning (ITL) [21] criterion called the maximum correntropy criterion (MCC) has been successfully applied to adaptive filters [22]–[24], randomized learning machines [25]–[29], principal component analysis (PCA) [30], auto-encoder [31], [32], common spatial patterns (CSP) [33], and many others. These successful applications demonstrate that MCC performs very well with outliers. In addition, according to *Property 3* provided in [34], correntropy has the potential to capture both the second-order and higher-order statistical characteristics of errors when the Gaussian kernel is used. With an appropriate setting of kernel size, the second-order statistical characteristics of errors can be dominant, which makes correntropy based optimization criterion also become a suitable choice for Gaussian noise or noise free environment. Inspired by the successful applications and attractive features of correntropy, we adopt it to train the output weights of BLS. Our main contributions are summarized as follows:

- By using an MCC based fixed-point iteration algorithm to train the output weights of BLS, we propose a correntropy based BLS (C-BLS). The new method is robust to outliers, and has the potential to achieve comparable performance to the standard BLS in Gaussian noise or noise free environment.
- Three alternative incremental learning algorithms that are derived from a weighted regularized least-squares solution rather than pseudoinverse formula are provided. These algorithms ensure that the system can be remodeled quickly without the entire retraining process from the beginning when some new samples arrive or the network deems to be expanded.
- To test the effectiveness of the proposed methods comprehensively, various regression and classification applications are provided for performance evaluation.

The remainder of the paper is organized as follows. In Section II, we give a brief review of BLS. In Section III, the correntropy is introduced, and based on correntropy, we propose the C-BLS and its incremental learning algorithms. Section IV presents experiment results on various regression and classification applications to demonstrate the performance of the proposed methods. At last, the conclusion is made in section V.

II. BROAD LEARNING SYSTEM

The basic idea of BLS comes from random vector functional-link neural networks (RVFLNN) [35], [36], but the direct connections between the input layer and the output layer of RVFLNN are replaced by a set of general mapped features, and the system can be flattened in the wide sense

by the enhancement nodes. Such deformation leads to some interesting properties and even makes BLS outperform several deep structure based learning methods [1], [5].

A. Basic Structure and Training Algorithm

Fig. 1 shows the basic architecture of BLS [1]. Herein, $\mathbf{X} = [\mathbf{x}_1^T, \mathbf{x}_2^T, \dots, \mathbf{x}_N^T]^T \in \mathbb{R}^{N \times M}$ and $\mathbf{Y} = [\mathbf{y}_1^T, \mathbf{y}_2^T, \dots, \mathbf{y}_N^T]^T \in \mathbb{R}^{N \times C}$ are respectively the input and the output matrices, where N denotes the number of samples, T represents the transpose operator, M is the dimension of each input vector, and C denotes the dimension of each output.

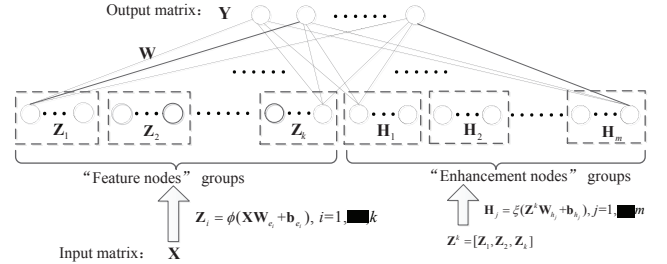


Fig. 1. The basic architecture of broad learning system.

Based on \mathbf{X} , k groups of mapped features denoted as $\mathbf{Z}_1, \mathbf{Z}_2, \dots, \mathbf{Z}_k$ are firstly obtained by

$$\mathbf{Z}_i = \phi_i(\mathbf{X}\mathbf{W}_{e_i} + \beta_{e_i}) \in \mathbb{R}^{N \times q}, \quad i = 1, 2, \dots, k \quad (1)$$

where ϕ_i is usually a linear transformation; q corresponds to the number of feature nodes in each group; $\mathbf{W}_{e_i} \in \mathbb{R}^{M \times q}$ and $\beta_{e_i} \in \mathbb{R}^{N \times q}$ are randomly generated weights and biases, respectively. In order to obtain the sparse representations of input data, they can be slightly fine-tuned by a sparse auto-encoder [1]. Concatenating all mapped features together, we have

$$\mathbf{Z}^k = [\mathbf{Z}_1, \mathbf{Z}_2, \dots, \mathbf{Z}_k] \in \mathbb{R}^{N \times kq}. \quad (2)$$

Based on \mathbf{Z}^k , m groups of “enhancement nodes” denoted as $\mathbf{H}_1, \mathbf{H}_2, \dots, \mathbf{H}_m$ are further obtained, that is

$$\mathbf{H}_j = \xi_j(\mathbf{Z}^k \mathbf{W}_{h_j} + \beta_{h_j}) \in \mathbb{R}^{N \times r}, \quad j = 1, 2, \dots, m \quad (3)$$

where ξ_j is an activation function, such as $\xi_j(x) = \tanh(x)$; r corresponds to the number of enhancement nodes in each group; $\mathbf{W}_{h_j} \in \mathbb{R}^{kq \times r}$ and $\beta_{h_j} \in \mathbb{R}^{N \times r}$ are also randomly generated weights and biases, respectively. These “enhancement nodes” can also be cascaded into one in the form of

$$\mathbf{H}^m = [\mathbf{H}_1, \mathbf{H}_2, \dots, \mathbf{H}_m] \in \mathbb{R}^{N \times mr}. \quad (4)$$

By concatenating \mathbf{Z}^k and \mathbf{H}^m , we obtain

$$\mathbf{U} = [\mathbf{Z}^k, \mathbf{H}^m] \in \mathbb{R}^{N \times L}, \quad (5)$$

where $L = kq + mr$. Clearly, \mathbf{U} is a new representation of the original input matrix \mathbf{X} , and termed as the state matrix in [10]. Since all $\{\mathbf{W}_{e_i}, \beta_{e_i}\}_{i=1}^k$ and $\{\mathbf{W}_{h_j}, \beta_{h_j}\}_{j=1}^m$ are randomly generated and remain unchanged after that, the learning task reduces to estimate the output weights \mathbf{W} . This optimization

problem can be modeled as to find the regularized least-squares solution of $\mathbf{Y} = \mathbf{U}\mathbf{W}$, that is

$$\arg \min_{\mathbf{W}} (\|\mathbf{U}\mathbf{W} - \mathbf{Y}\|_2^2 + \lambda \|\mathbf{W}\|_2^2). \quad (6)$$

Therefore, we have

$$\mathbf{W} = (\mathbf{U}^T\mathbf{U} + \lambda\mathbf{I})^{-1}\mathbf{U}^T\mathbf{Y}, \quad (7)$$

in which \mathbf{I} denotes an identify matrix with proper dimensions, and λ is a nonnegative constant for regularization. One should note that when $\lambda \rightarrow 0$, the solution in (7) is equivalent to

$$\mathbf{W} = \mathbf{U}^\dagger\mathbf{Y}, \quad (8)$$

where $\mathbf{U}^\dagger = \lim_{\lambda \rightarrow 0} (\mathbf{U}^T\mathbf{U} + \lambda\mathbf{I})^{-1}\mathbf{U}^T$ denotes the pseudoinverse of \mathbf{U} . Equation (8) has been chosen as the main strategy in [1] for finding the output weights \mathbf{W} .

B. Incremental Learning Algorithms for BLS

We now give a brief introduction to the incremental learning algorithms of BLS. For simplicity, the subscripts of the feature mapping ϕ_i and the activation function ξ_j will be omitted in the following, but one should note that ϕ_i can be selected differently in practice as well as ξ_j . In addition, we denote $\mathbf{X}(t)$ and $\mathbf{Y}(t)$ as the current input matrix and the current output matrix, respectively. According to (8), the current output weights can be obtained by

$$\mathbf{W}(t) = \mathbf{U}(t)^\dagger\mathbf{Y}(t). \quad (9)$$

where $\mathbf{U}(t)$ is the state matrix calculated according to (1)-(5). Obviously, to derive the incremental learning algorithms of BLS, we need to determine the new forms of $\mathbf{U}(t)$ and $\mathbf{Y}(t)$.

1) *Increment of New Samples:* When N_0 new samples $\{\mathbf{x}_i, \mathbf{y}_i\}_{i=N+1}^{N+N_0}$ arrive, the increased input matrix and output matrix can be expressed by $\mathbf{X}_\alpha = [\mathbf{x}_{N+1}^T, \dots, \mathbf{x}_{N+N_0}^T]^T \in \mathbb{R}^{N_0 \times M}$ and $\mathbf{Y}_\alpha = [\mathbf{y}_{N+1}^T, \dots, \mathbf{y}_{N+N_0}^T]^T \in \mathbb{R}^{N_0 \times C}$, respectively. The new state matrix and the output matrix are therefore obtained by

$$\mathbf{U}(t+1) = \begin{bmatrix} \mathbf{U}(t) \\ \mathbf{U}_\alpha \end{bmatrix}, \quad \mathbf{Y}(t+1) = \begin{bmatrix} \mathbf{Y}(t) \\ \mathbf{Y}_\alpha \end{bmatrix}, \quad (10)$$

where $\mathbf{U}_\alpha = [\mathbf{Z}_\alpha^k, \mathbf{H}_\alpha^m] \in \mathbb{R}^{N_0 \times L}$, and

$$\mathbf{Z}_\alpha^k = [\phi(\mathbf{X}_\alpha\mathbf{W}_{e_1} + \beta_{e_1}), \dots, \phi(\mathbf{X}_\alpha\mathbf{W}_{e_k} + \beta_{e_k})], \quad (11)$$

$$\mathbf{H}_\alpha^m = [\xi(\mathbf{Z}_\alpha^k\mathbf{W}_{h_1} + \beta_{h_1}), \dots, \xi(\mathbf{Z}_\alpha^k\mathbf{W}_{h_m} + \beta_{h_m})], \quad (12)$$

According to [1], [36], the pseudoinverse of $\mathbf{U}(t+1)$ in (10) can be calculated by

$$\mathbf{U}(t+1)^\dagger = [\mathbf{U}(t)^\dagger - \mathbf{B}\mathbf{D}, \mathbf{B}], \quad (13)$$

with

$$\begin{aligned} \mathbf{D} &= \mathbf{U}_\alpha\mathbf{U}(t)^\dagger \\ \mathbf{B} &= \begin{cases} \mathbf{C}^\dagger, & \text{if } \mathbf{C} \neq \mathbf{0} \\ (\mathbf{I} + \mathbf{D}\mathbf{D}^T)^{-1}\mathbf{D}^T\mathbf{U}(t)^\dagger\mathbf{D}^T, & \text{if } \mathbf{C} = \mathbf{0} \end{cases} \\ \mathbf{C} &= \mathbf{U}_\alpha - \mathbf{D}\mathbf{U}(t). \end{aligned} \quad (14)$$

Correspondingly, the update equation for the output weights has the following form

$$\begin{aligned} \mathbf{W}(t+1) &= \mathbf{U}(t+1)^\dagger\mathbf{Y}(t+1) \\ &= \mathbf{W}(t) + \mathbf{B}(\mathbf{Y}_\alpha - \mathbf{U}_\alpha\mathbf{W}(t)). \end{aligned} \quad (15)$$

2) *Increment of Enhancement Mapping Nodes:* When p new enhancement nodes are inserted, the state matrix changes to

$$\mathbf{U}(t+1) = [\mathbf{U}(t), \xi(\mathbf{Z}^k\mathbf{W}_{h_{m+1}} + \beta_{h_{m+1}})], \quad (16)$$

where $\mathbf{W}_{h_{m+1}} \in \mathbb{R}^{kq \times p}$ and $\beta_{h_{m+1}} \in \mathbb{R}^{N \times p}$ are randomly generated weights and biases, respectively. The pseudoinverse of $\mathbf{U}(t+1)$ in (16) can be calculated in the following way [1]

$$\mathbf{U}(t+1)^\dagger = \begin{bmatrix} \mathbf{U}(t+1)^\dagger - \mathbf{D}\mathbf{B}^T \\ \mathbf{B}^T \end{bmatrix}, \quad (17)$$

with

$$\begin{aligned} \mathbf{D} &= \mathbf{U}(t)^\dagger\xi(\mathbf{Z}^k\mathbf{W}_{h_{m+1}} + \beta_{h_{m+1}}) \\ \mathbf{B}^T &= \begin{cases} \mathbf{C}^\dagger, & \text{if } \mathbf{C} \neq \mathbf{0} \\ (\mathbf{I} + \mathbf{D}^T\mathbf{D})^{-1}\mathbf{D}^T\mathbf{U}(t)^\dagger, & \text{if } \mathbf{C} = \mathbf{0} \end{cases} \\ \mathbf{C} &= \xi(\mathbf{Z}^k\mathbf{W}_{h_{m+1}} + \beta_{h_{m+1}}) - \mathbf{U}(t)\mathbf{D}. \end{aligned} \quad (18)$$

Since $\mathbf{Y}(t+1) = \mathbf{Y}(t)$, the output weights in this case are therefore updated by

$$\mathbf{W}(t+1) = \mathbf{U}(t+1)^\dagger\mathbf{Y}(t+1) = \begin{bmatrix} \mathbf{W}(t) - \mathbf{D}\mathbf{B}^T\mathbf{Y}(t) \\ \mathbf{B}^T\mathbf{Y}(t) \end{bmatrix}. \quad (19)$$

3) *Increment of Feature Mapping Nodes:* When the $(k+1)$ th group of feature nodes are inserted, we have

$$\mathbf{U}(t+1) = [\mathbf{U}(t), \mathbf{Z}_{k+1}, \mathbf{H}_{\text{ex}_m}], \quad (20)$$

with

$$\mathbf{Z}_{k+1} = \phi(\mathbf{X}\mathbf{W}_{e_{k+1}} + \beta_{e_{k+1}}), \quad (21)$$

$$\mathbf{H}_{\text{ex}_m} = [\xi(\mathbf{Z}_{k+1}\mathbf{W}_{\text{ex}_1} + \beta_{\text{ex}_1}), \dots, \xi(\mathbf{Z}_{k+1}\mathbf{W}_{\text{ex}_m} + \beta_{\text{ex}_m})], \quad (22)$$

where $\{\mathbf{W}_{\text{ex}_i}, \beta_{\text{ex}_i}\}_{i=1}^m$ are also randomly generated weights and biases that connect new feature nodes to the enhancement nodes. With a similar procedure used from (17) to (19), the new output weights here can be calculated by

$$\mathbf{W}(t+1) = \begin{bmatrix} \mathbf{W}(t) - \mathbf{D}\mathbf{B}^T\mathbf{Y}(t) \\ \mathbf{B}^T\mathbf{Y}(t) \end{bmatrix}, \quad (23)$$

with

$$\begin{aligned} \mathbf{D} &= \mathbf{U}(t)^\dagger[\mathbf{Z}_{k+1}, \mathbf{H}_{\text{ex}_m}] \\ \mathbf{B}^T &= \begin{cases} \mathbf{C}^\dagger, & \text{if } \mathbf{C} \neq \mathbf{0} \\ (\mathbf{I} + \mathbf{D}^T\mathbf{D})^{-1}\mathbf{D}^T\mathbf{U}(t)^\dagger, & \text{if } \mathbf{C} = \mathbf{0} \end{cases} \\ \mathbf{C} &= [\mathbf{Z}_{k+1}, \mathbf{H}_{\text{ex}_m}] - \mathbf{U}(t)\mathbf{D}. \end{aligned} \quad (24)$$

Remark 1: When some new samples arrive or some new nodes are involved, the above three incremental learning algorithms can update the output weights of BLS without needing to run a complete training cycle, which ensures that the system can be remodeled quickly. However, these incremental learning algorithms require the regularization factor to tend to zero, so that the regularized least squares solution can well approximate the pseudo-inverse. This is, of course, not always the good choice, since the regularization factor plays an important role to improve the model's generalization ability in many practical applications. In the next section, several more general incremental learning algorithms under the BLS architecture will be provided.

III. CORRENTROPY BASED BROAD LEARNING SYSTEM

Although BLS has so many attractive features, its dependence on the second order statistical characteristics of errors makes it not a suitable choice in complicated noise environments, especially when data are disturbed by some outliers [9]. To offer a robust version of BLS, we introduce in this section the concept of correntropy, and based on correntropy, the C-BLS and its incremental learning algorithms are developed.

A. Correntropy

Correntropy [34] is a local similarity measure between two arbitrary random variables X and Y , defined by

$$V_\sigma(X, Y) = E[\kappa_\sigma(X, Y)], \quad (25)$$

where $E(\cdot)$ denotes the expectation operator, and $\kappa_\sigma(\cdot, \cdot)$ is a Mercer kernel [37] controlled by the kernel size σ . Without loss of generality, the Gaussian kernel defined as $\kappa_\sigma(x, y) = \frac{1}{\sqrt{2\pi}\sigma} \exp(-\frac{\|x-y\|^2}{2\sigma^2})$ will be a default choice in this paper. By using the Taylor series expansion to (25), we have

$$V_\sigma(X, Y) = \frac{1}{\sqrt{2\pi}\sigma} \sum_{n=1}^{\infty} \frac{(-1)^n}{2^n n!} E\left[\frac{(X-Y)^{2n}}{\sigma^{2n}}\right]. \quad (26)$$

Clearly, correntropy can be viewed as a weighted sum of all even moments of $X - Y$, and the weights of the second and higher-order moments are controlled by the kernel size σ . As δ increases, the high-order moments decay faster. Hence, the second-order moment has the chance to be dominant with a large σ . In practice, the data distribution is usually unknown and only a finite number of samples $\{(x_i, y_i)\}_{i=1}^N$ are available, resulting in the sample estimator of correntropy to be

$$\hat{V}_\sigma(X, Y) = \frac{1}{N} \sum_{i=1}^N \kappa_\sigma(x_i, y_i). \quad (27)$$

In signal processing and machine learning fields, it is usually to estimate an unknown parameter ω (such as the weight vector of an adaptive filter) by maximizing the correntropy between the desired signal Y and its estimated value \hat{Y} , i. e.,

$$\arg \max_{\omega} \hat{V}_\sigma(Y, \hat{Y}), \quad (28)$$

This optimization criterion is called MCC. Unlike the well known MMSE criterion which is sensitive to outliers, MCC has been proven to be very robust for parameters estimation in complicated noise environments [22], [23], [38]–[42].

B. Basic Training Algorithm for C-BLS

Similar to the standard BLS, the state matrix \mathbf{U} in the proposed method can be constructed through a series of feature mappings and enhancement transformations that have been described in (1)–(5). However, more powerful feature mapping strategies, such as convolution-pooling operation [5], neuro-fuzzy model [6], and structured manifold learning technology [7], are also feasible. Thus, the optimization model that combines BLS and MCC can be formulated by

$$\arg \max_{\mathbf{W}} \left(\sum_{i=1}^N \exp\left(-\frac{\|\mathbf{u}_i \mathbf{W} - \mathbf{y}_i\|_2^2}{2\sigma^2}\right) - \frac{\lambda}{2} \|\mathbf{W}\|_2^2 \right), \quad (29)$$

where $\mathbf{u}_i \in \mathbb{R}^L$ denotes the i th row of \mathbf{U} . For implicity, we denote $J(\mathbf{W}) = \sum_{i=1}^N \exp\left(-\frac{\|\mathbf{u}_i \mathbf{W} - \mathbf{y}_i\|_2^2}{2\sigma^2}\right) - \frac{\lambda}{2} \|\mathbf{W}\|_2^2$, and then (29) can be rewritten as

$$\arg \max_{\mathbf{W}} J(\mathbf{W}). \quad (30)$$

Taking the gradient of $J(\mathbf{W})$ with respect to \mathbf{W} , we have

$$\frac{\partial J(\mathbf{W})}{\partial \mathbf{W}} = -\frac{1}{\sigma^2} \sum_{i=1}^N \mathbf{u}_i^T \exp\left(-\frac{\|\mathbf{u}_i \mathbf{W} - \mathbf{y}_i\|_2^2}{2\sigma^2}\right) (\mathbf{u}_i \mathbf{W} - \mathbf{y}_i) - \lambda \mathbf{W}. \quad (31)$$

The matrix form of (31) can be expressed by

$$\frac{\partial J(\mathbf{W})}{\partial \mathbf{W}} = -\frac{1}{\sigma^2} \mathbf{U}^T \Lambda_w (\mathbf{U} \mathbf{W} - \mathbf{Y}) - \lambda \mathbf{W}, \quad (32)$$

with

$$\Lambda_w = \begin{bmatrix} \exp\left(-\frac{\|\mathbf{u}_1 \mathbf{W} - \mathbf{y}_1\|_2^2}{2\sigma^2}\right) & & \\ & \ddots & \\ & & \exp\left(-\frac{\|\mathbf{u}_N \mathbf{W} - \mathbf{y}_N\|_2^2}{2\sigma^2}\right) \end{bmatrix}. \quad (33)$$

By setting $\frac{\partial J(\mathbf{W})}{\partial \mathbf{W}}$ to zero, the solution of \mathbf{W} can be written in the following form

$$\mathbf{W} = (\mathbf{U}^T \Lambda_w \mathbf{U} + \gamma \mathbf{I})^{-1} \mathbf{U}^T \Lambda_w \mathbf{Y}, \quad (34)$$

where $\gamma = \lambda \sigma^2$. Obviously, Λ_w is the function of \mathbf{W} . Hence, (34) is actually a fixed-point equation which can be described by

$$\mathbf{W} = f(\mathbf{W}), \quad (35)$$

with

$$f(\mathbf{W}) = (\mathbf{U}^T \Lambda_w \mathbf{U} + \gamma \mathbf{I})^{-1} \mathbf{U}^T \Lambda_w \mathbf{Y}. \quad (36)$$

Referring to the widely used fixed-point iteration method [43]–[46], we can solve \mathbf{W} by the following iteration way

$$\mathbf{W}(t+1) = f(\mathbf{W}(t)), \quad (37)$$

where $\mathbf{W}(t)$ denotes the solution at iteration t . Let ε denote termination tolerance, the stopping criterion can be set as $\|\mathbf{W}(t+1) - \mathbf{W}(t)\|_2^2 < \varepsilon$. According to the work done in [44], the convergence of the fixed-point iteration method under the MCC can be guaranteed if the kernel size σ is appropriately chosen. In the following experiments, the grid search method will be adopted to determine σ and other parameters of C-BLS, so as to ensure its convergence and also make it approach its optimal performance as possible.

Finally, the proposed C-BLS is summarized in **Algorithm 1**.

Remark 2: Compared with (7) for the original BLS, (34) has an additive weighted diagonal matrix Λ_w , whose the i th diagonal element is controlled by the kernel size σ as well as the difference between \mathbf{y}_i and its estimation $\hat{\mathbf{y}}_i = \mathbf{u}_i \mathbf{W}$. It can be verified that when $\sigma \rightarrow \infty$, (34) will reduce to the solution of the standard BLS. This makes C-BLS can, at least, achieve the comparable performance to the standard BLS. In addition, by appropriately setting the values of σ , C-BLS has the potential to weaken the negative effects of outliers. For example, when the i th sample is polluted by outlier, there will be in general a large difference between \mathbf{y}_i and $\hat{\mathbf{y}}_i$, denoted

Algorithm 1: Correntropy Based Broad Learning System

Input: Training set $\{\mathbf{X}, \mathbf{Y}\}$.

Output: Output weight matrix \mathbf{W} .

1. **Parameters setting:** network parameters k, q, m, r , regularization parameter γ , kernel size σ , termination tolerance ε , maximum iteration number T .
 2. **Initialization:** set \mathbf{W}_0 and construct the state matrix \mathbf{U} according to (1)-(5).
 3. **for** $t = 1, \dots, T$ **do**
 4. Compute Λ_w according to (33);
 6. Update \mathbf{W} according to (34);
 7. Until $\|\mathbf{W}(t+1) - \mathbf{W}(t)\|_2^2 < \varepsilon$.
 8. **end for**
-

as $\nu = \|\mathbf{y}_i - \hat{\mathbf{y}}_i\|_2^2$. With appropriately setting of σ , such as $\sigma \rightarrow 0$, we have $\exp(-\frac{\nu}{2\sigma^2}) \rightarrow 0$, which makes the outlier not have a big impact on the training process.

Remark 3: The update equations of the proposed C-BLS is somewhat similar to the W-BLS proposed in [18]. However, there are several dissimilarities between them, including: 1) C-BLS is proposed from the Information Theoretic Learning ITL [21] perspective while W-BLS is proposed from the application of industrial process; 2) the weighted operator in C-BLS is a successive result derived from MCC while the weighted operator in W-BLS is an additional hyperparameter needed to be specified in advance; 3) C-BLS remains the connections between the input layer and the feature layer and hence can be easily combined with some existing feature mapping technologies [1], [5]–[7] while W-BLS abandons such connections.

C. Incremental Learning Algorithms for C-BLS

To derive the incremental learning algorithms of C-BLS, we also use $\mathbf{X}(t)$ and $\mathbf{Y}(t)$ to denote the current input matrix and the current output matrix, respectively. According to (34), we therefore get that

$$\begin{aligned} \mathbf{W}(t) &= [\mathbf{U}(t)^T \Lambda_{w(t)} \mathbf{U}(t) + \gamma \mathbf{I}]^{-1} \mathbf{U}(t)^T \Lambda_{w(t)} \mathbf{Y}(t) \\ &= (\mathbf{U}_{w(t)}^T \mathbf{U}_{w(t)} + \gamma \mathbf{I})^{-1} \mathbf{U}_{w(t)}^T \mathbf{Y}_{w(t)}, \end{aligned} \quad (38)$$

where $\mathbf{U}_{w(t)} = \sqrt{\Lambda_{w(t)}} \mathbf{U}(t)$ is the weighted state matrix, $\mathbf{Y}_{w(t)} = \sqrt{\Lambda_{w(t)}} \mathbf{Y}(t)$ corresponds to the weighted output matrix, and $\Lambda_{w(t)}$ is calculated by

$$\Lambda_{w(t)} = \begin{bmatrix} \exp(-\frac{\|\mathbf{u}_1 \mathbf{W}(t) - \mathbf{y}_1\|_2^2}{2\sigma^2}) & & \\ & \ddots & \\ & & \exp(-\frac{\|\mathbf{u}_N \mathbf{W}(t) - \mathbf{y}_N\|_2^2}{2\sigma^2}) \end{bmatrix}. \quad (39)$$

For ease of representation, we define $\mathbf{R}_{w(t)} = \mathbf{U}_{w(t)}^T \mathbf{U}_{w(t)} + \gamma \mathbf{I}$ and $\mathbf{P}_{w(t)} = \mathbf{U}_{w(t)}^T \mathbf{Y}_{w(t)}$. Hence, (38) can be written as

$$\mathbf{W}(t) = \mathbf{R}_{w(t)}^{-1} \mathbf{P}_{w(t)}. \quad (40)$$

1) *Increment of new samples:* Assume that N_0 new samples $\{\mathbf{x}_i, \mathbf{y}_i\}_{i=N+1}^{N+N_0}$ are available. We first denote $\mathbf{X}_\alpha = [\mathbf{x}_{N+1}^T, \dots, \mathbf{x}_{N+N_0}^T]^T \in \mathbb{R}^{N_0 \times M}$ and $\mathbf{Y}_\alpha = [\mathbf{y}_{N+1}^T, \dots, \mathbf{y}_{N+N_0}^T]^T \in \mathbb{R}^{N_0 \times C}$. Then, the weighted state matrix and output matrix can be obtained by

$$\mathbf{U}_{w(t+1)} \approx \begin{bmatrix} \mathbf{U}_{w(t)} \\ \mathbf{U}_\alpha \end{bmatrix}, \quad \mathbf{Y}_{w(t+1)} \approx \begin{bmatrix} \mathbf{Y}_{w(t)} \\ \mathbf{Y}_\alpha \end{bmatrix}, \quad (41)$$

where $\mathbf{U}_{w(t)}^\alpha = [\mathbf{Z}_{w(t)}^k, \mathbf{H}_{w(t)}^m] \in \mathbb{R}^{N_0 \times L}$ and $\mathbf{Y}_{w(t)}^\alpha = \sqrt{\Lambda_{w(t)}^\alpha} \mathbf{Y}_\alpha \in \mathbb{R}^{N_0 \times C}$ with

$$\Lambda_{w(t)}^\alpha = \begin{bmatrix} \exp(-\frac{\|\mathbf{u}_{N+1} \mathbf{W}(t) - \mathbf{y}_{N+1}\|_2^2}{2\sigma^2}) & & \\ & \ddots & \\ & & \exp(-\frac{\|\mathbf{u}_{N+N_0} \mathbf{W}(t) - \mathbf{y}_{N+N_0}\|_2^2}{2\sigma^2}) \end{bmatrix}, \quad (42)$$

$$\mathbf{Z}_{w(t)}^k = \sqrt{\Lambda_{w(t)}^\alpha} [\phi(\mathbf{X}_\alpha \mathbf{W}_{e_1} + \beta_{e_1}), \dots, \phi(\mathbf{X}_\alpha \mathbf{W}_{e_k} + \beta_{e_k})], \quad (43)$$

$$\mathbf{H}_{w(t)}^m = \sqrt{\Lambda_{w(t)}^\alpha} [\xi(\mathbf{Z}_\alpha^k \mathbf{W}_{h_1} + \beta_{h_1}), \dots, \xi(\mathbf{Z}_\alpha^k \mathbf{W}_{h_m} + \beta_{h_m})]. \quad (44)$$

Substituting $\mathbf{U}_{w(t+1)}$ and $\mathbf{Y}_{w(t+1)}$ into (40), we have

$$\mathbf{W}(t+1) = \mathbf{R}_{w(t+1)}^{-1} \mathbf{P}_{w(t+1)}, \quad (45)$$

where

$$\begin{aligned} \mathbf{R}_{w(t+1)} &= \mathbf{U}_{w(t+1)}^T \mathbf{U}_{w(t+1)} + \gamma \mathbf{I} \\ &\approx \begin{bmatrix} \mathbf{U}_{w(t)} \\ \mathbf{U}_\alpha \end{bmatrix}^T \begin{bmatrix} \mathbf{U}_{w(t)} \\ \mathbf{U}_\alpha \end{bmatrix} + \gamma \mathbf{I} \\ &= \mathbf{R}_{w(t)} + \mathbf{U}_{w(t)}^\alpha{}^T \mathbf{U}_{w(t)}^\alpha, \end{aligned} \quad (46)$$

and

$$\begin{aligned} \mathbf{P}_{w(t+1)} &= \mathbf{U}_{w(t+1)}^T \mathbf{Y}_{w(t+1)} \\ &\approx \begin{bmatrix} \mathbf{U}_{w(t)} \\ \mathbf{U}_\alpha \end{bmatrix}^T \begin{bmatrix} \mathbf{Y}_{w(t)} \\ \mathbf{Y}_\alpha \end{bmatrix} \\ &= \mathbf{P}_{w(t)} + \mathbf{U}_{w(t)}^\alpha{}^T \mathbf{Y}_{w(t)}^\alpha. \end{aligned} \quad (47)$$

By using the matrix inverse lemma

$$(\mathbf{A} + \mathbf{BCD})^{-1} = \mathbf{A}^{-1} - \mathbf{A}^{-1} \mathbf{B} (\mathbf{C}^{-1} + \mathbf{D} \mathbf{A}^{-1} \mathbf{B})^{-1} \mathbf{D} \mathbf{A}^{-1} \quad (48)$$

with the definitions of $\mathbf{A} = \mathbf{R}_{w(t)}$, $\mathbf{B} = \mathbf{U}_{w(t)}^\alpha{}^T$, $\mathbf{C} = \mathbf{I}$ and $\mathbf{D} = \mathbf{U}_{w(t)}^\alpha$, we get

$$\mathbf{R}_{w(t+1)}^{-1} = \mathbf{R}_{w(t)}^{-1} - \mathbf{R}_{w(t)}^{-1} \mathbf{U}_{w(t)}^\alpha{}^T \mathbf{S}_{w(t)}^\alpha \mathbf{U}_{w(t)}^\alpha \mathbf{R}_{w(t)}^{-1}, \quad (49)$$

where $\mathbf{S}_{w(t)}^\alpha = [\mathbf{I} + \mathbf{U}_{w(t)}^\alpha{}^T \mathbf{R}_{w(t)}^{-1} \mathbf{U}_{w(t)}^\alpha]^{-1}$. Substituting (47) and (49) into (45), yields

$$\begin{aligned} \mathbf{W}(t+1) &= \mathbf{R}_{w(t+1)}^{-1} \mathbf{P}_{w(t+1)} \\ &= \mathbf{W}(t) + \mathbf{R}_{w(t)}^{-1} \mathbf{U}_{w(t)}^\alpha{}^T \mathbf{S}_{w(t)}^\alpha (\mathbf{Y}_{w(t)}^\alpha - \mathbf{U}_{w(t)}^\alpha \mathbf{W}(t)). \end{aligned} \quad (50)$$

Let $\mathbf{C}_{w(t)} = \mathbf{R}_{w(t)}^{-1}$. We obtain the final equations for updating $\mathbf{W}(t+1)$ as follows

$$\begin{aligned} \mathbf{S}_{w(t)}^\alpha &= [\mathbf{I} + \mathbf{U}_{w(t)}^\alpha{}^T \mathbf{C}_{w(t)} \mathbf{U}_{w(t)}^\alpha]^{-1} \\ \mathbf{W}(t+1) &= \mathbf{W}(t) + \mathbf{C}_{w(t)} \mathbf{U}_{w(t)}^\alpha{}^T \mathbf{S}_{w(t)}^\alpha (\mathbf{Y}_{w(t)}^\alpha - \mathbf{U}_{w(t)}^\alpha \mathbf{W}(t)) \\ \mathbf{C}_{w(t+1)} &= \mathbf{C}_{w(t)} - \mathbf{C}_{w(t)} \mathbf{U}_{w(t)}^\alpha{}^T \mathbf{S}_{w(t)}^\alpha \mathbf{U}_{w(t)}^\alpha \mathbf{C}_{w(t)}. \end{aligned} \quad (51)$$

The main computational effort in (51) focuses on the calculation of $\mathbf{S}_{w(t)}^\alpha$. Since only the latest N_0 samples as well as the previous $\mathbf{C}_{w(t)}$ are involved to compute $\mathbf{S}_{w(t)}^\alpha$, the corresponding computational cost is in general not burdensome.

2) *Increment of Enhancement Nodes*: Assume that p enhancement nodes are inserted. The weighted state matrix can be expressed by

$$\mathbf{U}_{w(t+1)} \approx [\mathbf{U}_{w(t)}, \xi_{w(t)}], \quad (52)$$

where $\xi_{w(t)} = \sqrt{\Lambda_{w(t)}} \xi(\mathbf{Z}^k \mathbf{W}_{h_{m+1}} + \beta_{h_{m+1}}) \in \mathbb{R}^{N \times p}$; $\mathbf{W}_{h_{m+1}} \in \mathbb{R}^{kq \times p}$ and $\beta_{h_{m+1}} \in \mathbb{R}^{N \times p}$ are randomly generated weights and biases, respectively. With the approximation of $\mathbf{Y}_{w(t+1)} \approx \mathbf{Y}_{w(t)}$, the output weights in this case are obtained by

$$\mathbf{W}(t+1) = \mathbf{R}_{w(t+1)}^{-1} \mathbf{P}_{w(t+1)}, \quad (53)$$

with

$$\begin{aligned} \mathbf{R}_{w(t+1)} &= \mathbf{U}_{w(t+1)}^T \mathbf{U}_{w(t+1)} + \gamma \mathbf{I} \\ &\approx \begin{bmatrix} \mathbf{U}_{w(t)}^T \\ \xi_{w(t)}^T \end{bmatrix} [\mathbf{U}_{w(t)}, \xi_{w(t)}] + \gamma \mathbf{I} \\ &= \begin{bmatrix} \mathbf{R}_{w(t)} & \mathbf{U}_{w(t)}^T \xi_{w(t)} \\ \xi_{w(t)}^T \mathbf{U}_{w(t)} & \gamma \mathbf{I} + \xi_{w(t)}^T \xi_{w(t)} \end{bmatrix}, \end{aligned} \quad (54)$$

and

$$\begin{aligned} \mathbf{P}_{w(t+1)} &= \mathbf{U}_{w(t+1)}^T \mathbf{Y}_{w(t+1)} \\ &\approx \begin{bmatrix} \mathbf{U}_{w(t)}^T \\ \xi_{w(t)}^T \end{bmatrix} \mathbf{Y}_{w(t)} \\ &= \begin{bmatrix} \mathbf{P}_{w(t)} \\ \xi_{w(t)}^T \mathbf{Y}_{w(t)} \end{bmatrix}, \end{aligned} \quad (55)$$

The inverse matrix of $\mathbf{R}_{w(t+1)}$ in (53) can be calculated by using the block matrix inversion lemma [47], which has the form of

$$\begin{bmatrix} \mathbf{A} & \mathbf{B} \\ \mathbf{C} & \mathbf{D} \end{bmatrix}^{-1} = \begin{bmatrix} (\mathbf{A} - \mathbf{B}\mathbf{D}^{-1}\mathbf{C})^{-1} & -\mathbf{A}^{-1}\mathbf{B}(\mathbf{D} - \mathbf{C}\mathbf{A}^{-1}\mathbf{B})^{-1} \\ -(\mathbf{D} - \mathbf{C}\mathbf{A}^{-1}\mathbf{B})^{-1}\mathbf{C}\mathbf{A}^{-1} & (\mathbf{D} - \mathbf{C}\mathbf{A}^{-1}\mathbf{B})^{-1} \end{bmatrix}, \quad (56)$$

where \mathbf{A} and \mathbf{D} are arbitrary reversible matrix blocks. Let $\mathbf{A} = \mathbf{R}_{w(t)}$, $\mathbf{B} = \mathbf{U}_{w(t)}^T \xi_{w(t)}$, $\mathbf{C} = \xi_{w(t)}^T \mathbf{U}_{w(t)}$, and $\mathbf{D} = \gamma \mathbf{I} + \xi_{w(t)}^T \xi_{w(t)}$, then we get

$$\mathbf{R}_{w(t+1)}^{-1} = \begin{bmatrix} \mathbf{R}_{w(t)}^{-1} + \mathbf{Z}_{w(t)} \mathbf{Q}_{w(t)} \mathbf{Z}_{w(t)}^T & -\mathbf{Z}_{w(t)} \mathbf{Q}_{w(t)} \\ -\mathbf{Q}_{w(t)} \mathbf{Z}_{w(t)}^T & \mathbf{Q}_{w(t)} \end{bmatrix}, \quad (57)$$

where

$$\begin{aligned} \mathbf{Z}_{w(t)} &= \mathbf{R}_{w(t)}^{-1} \mathbf{U}_{w(t)}^T \xi_{w(t)}, \\ \mathbf{Q}_{w(t)} &= \left(\gamma \mathbf{I} + \xi_{w(t)}^T \xi_{w(t)} - \xi_{w(t)}^T \mathbf{U}_{w(t)} \mathbf{Z}_{w(t)} \right)^{-1}. \end{aligned} \quad (58)$$

Substituting (56) and (57) into (53), we have

$$\begin{aligned} \mathbf{W}(t+1) &= \mathbf{R}_{w(t+1)}^{-1} \mathbf{P}_{w(t+1)} \\ &= \begin{bmatrix} \mathbf{W}(t) - \mathbf{Z}_{w(t)} \mathbf{Q}_{w(t)} \xi_{w(t)}^T (\mathbf{Y}_{w(t)} - \mathbf{U}_{w(t)} \mathbf{W}(t)) \\ \mathbf{Q}_{w(t)} \xi_{w(t)}^T (\mathbf{Y}_{w(t)} - \mathbf{U}_{w(t)} \mathbf{W}(t)) \end{bmatrix}. \end{aligned} \quad (59)$$

3) *Increment of Feature Mapping Nodes*: Assume that the $(k+1)$ th group of feature nodes are inserted. The new weighted state matrix can be constructed by

$$\mathbf{U}_{w(t+1)} \approx [\mathbf{U}_{w(t)}, \vartheta_{w(t)}], \quad (60)$$

where $\vartheta_{w(t)} = [\mathbf{Z}_{w(t)}, \mathbf{H}_{w(t)}]$ with

$$\mathbf{Z}_{w(t)} = \sqrt{\Lambda_{w(t)}} \phi(\mathbf{X} \mathbf{W}_{e_{k+1}} + \beta_{e_{k+1}}), \quad (61)$$

$$\mathbf{H}_{w(t)} = \sqrt{\Lambda_{w(t)}} [\xi(\mathbf{Z}_{k+1} \mathbf{W}_{e_{x_1}} + \beta_{e_{x_1}}), \dots, \xi(\mathbf{Z}_{k+1} \mathbf{W}_{e_{x_m}} + \beta_{e_{x_m}})]. \quad (62)$$

Herein, $\{\mathbf{W}_{e_{x_i}}, \beta_{e_{x_i}}\}_{i=1}^m$ are weights and biases, which are also randomly generated. Similar to the case of increasing enhancement nodes, we get the update equation for the output weights as

$$\begin{aligned} \mathbf{W}(t+1) &= \mathbf{R}_{w(t+1)}^{-1} \mathbf{P}_{w(t+1)} \\ &= \begin{bmatrix} \mathbf{W}(t) - \mathbf{Z}_{w(t)} \mathbf{Q}_{w(t)} \vartheta_{w(t)}^T (\mathbf{Y}_{w(t)} - \mathbf{U}_{w(t)} \mathbf{W}(t)) \\ \mathbf{Q}_{w(t)} \vartheta_{w(t)}^T (\mathbf{Y}_{w(t)} - \mathbf{U}_{w(t)} \mathbf{W}(t)) \end{bmatrix}, \end{aligned} \quad (63)$$

where

$$\begin{aligned} \mathbf{Z}_{w(t)} &= \mathbf{R}_{w(t)}^{-1} \mathbf{U}_{w(t)}^T \vartheta_{w(t)}, \\ \mathbf{Q}_{w(t)} &= \left(\gamma \mathbf{I} + \vartheta_{w(t)}^T \vartheta_{w(t)} - \vartheta_{w(t)}^T \mathbf{U}_{w(t)} \mathbf{Z}_{w(t)} \right)^{-1} \\ \mathbf{R}_{w(t+1)}^{-1} &= \begin{bmatrix} \mathbf{R}_{w(t)}^{-1} + \mathbf{Z}_{w(t)} \mathbf{Q}_{w(t)} \mathbf{Z}_{w(t)}^T & -\mathbf{Z}_{w(t)} \mathbf{Q}_{w(t)} \\ -\mathbf{Q}_{w(t)} \mathbf{Z}_{w(t)}^T & \mathbf{Q}_{w(t)} \end{bmatrix}. \end{aligned} \quad (64)$$

Remark 4: It is clear that all the incremental learning algorithms proposed in this section support the fast re-modeling, since the main computational efforts in them focus on the calculations of the additional part rather than the whole body of weighted auto-correlation matrix $\mathbf{R}_{w(t+1)}$. In addition, we don't restrict that the regularization factor tends to zero in all derivation processes, which makes them have the potential to get a better generalization in practice. Thus, they can be viewed as general incremental learning algorithms under the BLS architecture.

IV. EXPERIMENT RESULTS

In this section, the experiments are presented to demonstrate the desirable performance of the proposed C-BLS and its incremental learning algorithms. Except mentioned otherwise, all the experiment results are obtained using MATLAB (R2017b) on a 3.60-GHz machine with 16-GB RAM.

A. Performance Evaluation of C-BLS

Thirteen benchmark datasets, seven of which are for regression and the other six are for classification, from the UCI repository [48] are adopted here to evaluate the performance of C-BLS. The details of these datasets are shown in Table I, in which the symbol '#' represents the value of a variable or the number of samples in a set, and the symbol '-' means that the dataset is used for regression only. To eliminate the influence of data scales, both input and output attributes for regression datasets are normalized into the range $[0, 1]$, while for classification datasets, only the input attributes are normalized into the range $[-1, 1]$.

1) *Comparison with the Standard BLS*: First, we compare the performance of C-BLS with the standard BLS on the aforementioned thirteen datasets. There are several common parameters for BLS and C-BLS, including the number of feature nodes N_f , the number of mapping groups N_m , the number of enhancement nodes N_e , and the regularization factor γ . Similar to [5], we simply set the regularization factor to $\gamma = 2^{-30}$, and perform a grid search on the best combination of N_f , N_w and N_e . In detail, the search ranges for N_f is $[1, 20]$ with the step-size of 2, for N_w is $[1, 20]$ with the step-size of 1, and for N_e is $[1, 200]$ with the step-size of

TABLE I
SPECIFICATION OF THE FOURTEEN BENCHMARK DATA SETS.

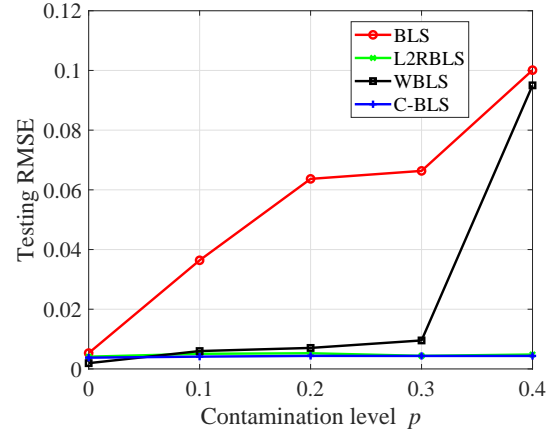
Dataset	#Class	#Attributes	#Training	#Testing
Airfoil Self-Noise	-	5	1002	501
Bodyfat	-	14	168	84
Cleveland	-	13	202	101
Forestfires	-	12	345	172
Mortgage	-	15	699	350
Quake	-	3	1452	726
Weather Izmir	-	9	974	487
Balance Scale	3	4	417	208
Chess	2	36	2131	1065
Diabetes	2	8	512	256
Ecoli	8	7	222	114
Horse Colic	2	27	300	68
Wireless	4	7	1332	668

5. As for the kernel size introduced in C-BLS, it is searched in the range of $\{2^{-5}, 2^{-4}, \dots, 2^4, 2^5\}$.

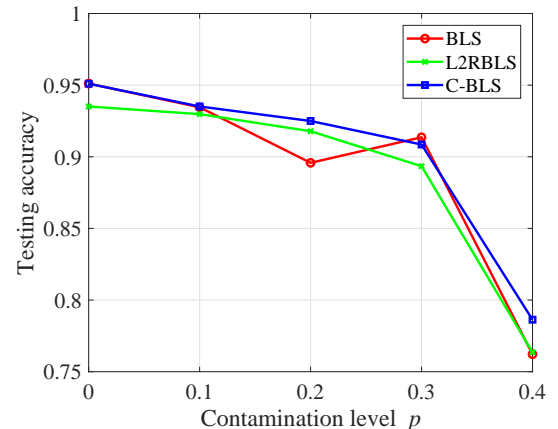
Table II and Table III show the comparative results of BLS and C-BLS on regression and classification datasets, respectively. To reduce the random error caused by experiment itself, all the results have been averaged over 20 Monte Carlo runs. It can be seen from Table II that, except for the dataset “Forestfires”, C-BLS can always reach a smaller or the same testing root mean square error (RMSE) [7] compared with the standard BLS. Furthermore, the comparative results on Table II shows that, even applied to classification tasks, C-BLS also have the ability to get the same or a higher testing accuracy on most of datasets. However, C-BLS in general needs more training time compared with the standard BLS, since there is no closed-solution under MCC. To reduce the time consuming, one can adopt some existing technologies, like single-value-decomposition (SVD) technology [9], [49] or just providing a good initialization [24] for speeding up the calculation. Due to space limitation, we don’t give a through discussion here.

2) *Comparison with Robust BLS Variants:* Although C-BLS, in general, performs better than the standard BLS in the aforementioned thirteen data sets in terms of testing RMSE or testing accuracy, it is hard to say that C-BLS is robust to outliers, since we don’t know any prior information about the noise distribution of these real datasets. To test the robustness of C-BLS, we choose the dataset “Bodyfat” and the dataset “Chess” as two representative examples. In detail, for dataset “Bodyfat”, the targets of training samples are added with random outliers from the interval $[0, 1]$, with the contamination level of p ; for dataset “Chess”, a part of training samples (with the ratio of p) are randomly selected and their class labels are reversed to its opposite side. Moreover, we note that there are several robust BLS variants that are also realized by replacing the MMSE criterion with other robust one, i. e, the robust BLS with l_2 -norm regularization (L2RBLS) [9] and the weighted BLS (WBLS) [18]. Therefore, not only the standard BLS but also these two methods are chosen as the benchmarks for comparison. To make all comparative algorithms reach their best performance as much as possible, we also perform a grid

search for their parameters. In detail, all the aforementioned parameters search ranges of the standard BLS are shared with L2RBLS since they share the same architecture with each other. For WBLS, the Huber weight function with cut-value b being chosen from $\{0.1, 0.3, 0.5, 0.7, 1, 3, 5, 7, 10\}$ is adopted as the weighted penalty factor and the regularization parameter is fixed at 2^{-30} . Then, we search its optimal number of enhancement nodes from $[1, 600]$ with the step-size of 10.



(a) Regression dataset: Bodyfat



(b) Classification dataset: Chess

Fig. 2. Performance comparison of different algorithms under different contamination level p .

Fig. 2 shows the comparative results of different methods versus contamination level p . It can be seen from Fig. 2(a) that, with the increment of p , the testing RMSE of BLS increases evidently while the testing RMSEs of L2RBLS, WBLS and C-BLS are not very sensitive to p . Moreover, the proposed C-BLS can, in general, achieve a smaller testing RMSE compared with L2RBLS and WBLS. Similarly, we can see from Fig. 2(b) that, the proposed C-BLS also performs better than others when applied to classification tasks. It is worth noting that the weighted operators provided in [18] are originally designed for multiple-input-single-output regression cases, so we don’t apply the corresponding WBLS to classification datasets in this part. Moreover, the robustness of C-BLS seems to be not as strong as those in regression examples, since its testing accuracy decreases evidently like the standard

TABLE II
PERFORMANCE COMPARISON OF BLS AND C-BLS ON REGRESSION BENCHMARK DATA SETS

Dataset	Algorithm	Parameters	Training Time (s)	Training RMSE	Testing RMSE
Airfoil Self-Noise	BLS	$(N_f, N_w, N_e) = (1, 5, 166)$	0.0094 ± 0.0012	0.0651 ± 0.0045	0.0959 ± 0.0137
	C-BLS	$(N_f, N_w, N_e, \sigma) = (1, 20, 136, 2^{-2})$	0.1099 ± 0.0047	0.0674 ± 0.0022	0.0923 ± 0.0074
Bodyfat	BLS	$(N_f, N_w, N_e) = (13, 17, 1)$	0.0151 ± 0.0019	0.0080 ± 0.0001	0.0054 ± 0.0001
	C-BLS	$(N_f, N_w, N_e, \sigma) = (3, 12, 21, 2^{-5})$	0.0161 ± 0.0047	0.0073 ± 0.0007	0.0040 ± 0.0007
Cleveland	BLS	$(N_f, N_w, N_e) = (1, 1, 151)$	0.0020 ± 0.0004	0.1106 ± 0.0011	0.1312 ± 0.0100
	C-BLS	$(N_f, N_w, N_e, \sigma) = (1, 1, 21, 2^{-1})$	0.0179 ± 0.0017	0.1104 ± 0.0013	0.1306 ± 0.0076
Forestfires	BLS	$(N_f, N_w, N_e) = (1, 1, 1)$	0.0010 ± 0.0001	0.0593 ± 0.0001	0.0561 ± 0.0001
	C-BLS	$(N_f, N_w, N_e, \sigma) = (1, 1, 1, 2^{-3})$	0.0020 ± 0.0002	0.0595 ± 0.0000	0.0563 ± 0.0001
Mortgage	BLS	$(N_f, N_w, N_e) = (3, 9, 141)$	0.0107 ± 0.0010	0.0030 ± 0.0001	0.0056 ± 0.0003
	C-BLS	$(N_f, N_w, N_e, \sigma) = (3, 9, 141, 2^{-4})$	0.0784 ± 0.0029	0.0030 ± 0.0001	0.0056 ± 0.0003
Quake	BLS	$(N_f, N_w, N_e) = (19, 19, 1)$	0.0378 ± 0.0023	0.1711 ± 0.0002	0.1728 ± 0.0003
	C-BLS	$(N_f, N_w, N_e, \sigma) = (19, 19, 1, 2^1)$	0.2364 ± 0.1275	0.1711 ± 0.0002	0.1728 ± 0.0003
Weather Izmir	BLS	$(N_f, N_w, N_e) = (3, 9, 31)$	0.0081 ± 0.0006	0.0175 ± 0.0003	0.0206 ± 0.0004
	C-BLS	$(N_f, N_w, N_e, \sigma) = (1, 16, 56, 2^{-5})$	0.0548 ± 0.0026	0.0173 ± 0.0011	0.0200 ± 0.0005

TABLE III
PERFORMANCE COMPARISON OF BLS AND C-BLS ON CLASSIFICATION BENCHMARK DATASETS

Dataset	Algorithm	Parameters	Training Time (s)	Training Accuracy	Testing Accuracy
Balance Scale	BLS	$(N_f, N_w, N_e) = (1, 11, 31)$	0.0079 ± 0.0004	91.34 ± 0.38	90.70 ± 1.00
	C-BLS	$(N_f, N_w, N_e, \sigma) = (1, 18, 41, 2^4)$	0.0401 ± 0.0027	91.94 ± 0.51	90.63 ± 1.10
Chess	BLS	$(N_f, N_w, N_e) = (3, 12, 176)$	0.0255 ± 0.0015	97.10 ± 0.43	95.44 ± 0.59
	C-BLS	$(N_f, N_w, N_e, \sigma) = (3, 12, 176, 2^5)$	0.0452 ± 0.0040	97.10 ± 0.43	95.44 ± 0.59
Diabetes	BLS	$(N_f, N_w, N_e) = (3, 12, 6)$	0.0090 ± 0.0004	79.04 ± 0.66	75.68 ± 1.03
	C-BLS	$(N_f, N_w, N_e, \sigma) = (7, 16, 6, 2^1)$	0.0566 ± 0.0027	79.27 ± 0.50	75.92 ± 1.02
Ecoli	BLS	$(N_f, N_w, N_e) = (1, 9, 11)$	0.0063 ± 0.0003	89.91 ± 0.68	86.18 ± 2.03
	C-BLS	$(N_f, N_w, N_e, \sigma) = (1, 9, 11, 2^5)$	0.0221 ± 0.0048	89.91 ± 0.68	86.18 ± 2.03
Horse Colic	BLS	$(N_f, N_w, N_e) = (17, 17, 21)$	0.0166 ± 0.0010	89.67 ± 0.87	80.81 ± 2.68
	C-BLS	$(N_f, N_w, N_e, \sigma) = (11, 13, 1, 2^4)$	0.0501 ± 0.0025	88.87 ± 0.23	82.21 ± 0.66
Wireless	BLS	$(N_e, N_f, N_e) = (5, 8, 161)$	0.0157 ± 0.0010	98.46 ± 0.18	97.53 ± 0.44
	C-BLS	$(N_e, N_f, N_e, \sigma) = (5, 8, 161, 2^3)$	0.1696 ± 0.0044	98.43 ± 0.17	97.56 ± 0.44

BLS and L2RBLs when $p = 0.4$. A possible reason is that the error distribution in classification applications is rather complicated compared to these multiple-input-single-output regression examples.

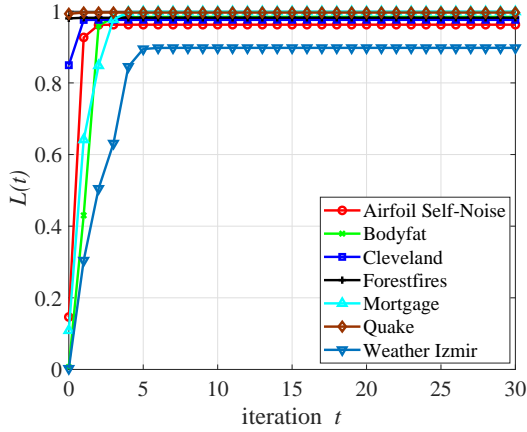
3) *Convergence Curves*: We now investigate the convergence of the proposed C-BLS. For this purpose, the value of the normalized objective function at iteration t is calculated by

$$L(t) = \frac{1}{N} \left(\sum_{i=1}^N \exp\left(-\frac{\|\mathbf{u}_i \mathbf{W}(t) - \mathbf{y}_i\|_2^2}{2\sigma^2}\right) - \frac{\lambda}{2} \|\mathbf{W}(t)\|_2^2 \right). \quad (65)$$

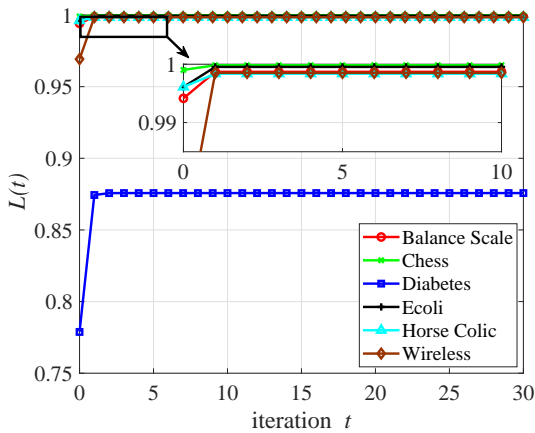
If the value of $L(t)$ is not decreasing, the convergence of the proposed C-BLS will be guaranteed. Fig. 3 shows the variation of the normalized objective function $L(t)$ versus iteration t . Herein, all parameters are set as the same of those in Tables II and III. It can be seen from Fig 3(a) and Fig 3(b) that, the value of $L(t)$ increases at the beginning and finally reach a stable value. This conforms the convergence of the proposed

C-BLS in our experiments. In addition, the stable value of C-BLS can be reached within 10 iterations for most datasets. Thus, the number of maximum iteration may be not necessary set to be a very large value for practical applications.

4) *Parameters Sensitivity*: Compared with the standard BLS, an additional parameter, i. e., kernel size σ , is introduced in C-BLS. In this subsection, the influence of σ on the learning performance of C-BLS is investigated. Therefore, we change the value of σ in a candidate set $\{2^{-7}, 2^{-6}, \dots, 2^6, 2^7\}$, while other parameters are determined in the same way detailed before. Fig. 4(a) and Fig. 4(b), respectively, show the testing RMSEs and testing accuracies on regression and classification datasets. As can be seen from Fig. 4(a) and Fig. 4(b), although the influence of σ on learning performance varies with datasets, there is always a range of σ in which the C-BLS performs better than others when a specific dataset is considered. Hence, σ is a parameter that should be appropriately chosen



(a) Regression datasets



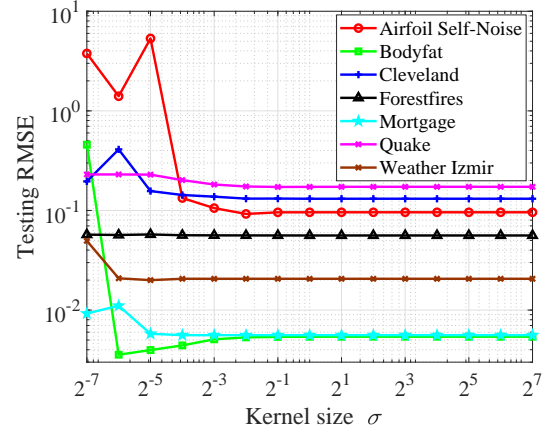
(b) Classification datasets

Fig. 3. Convergence curves of C-BLS on benchmark datasets.

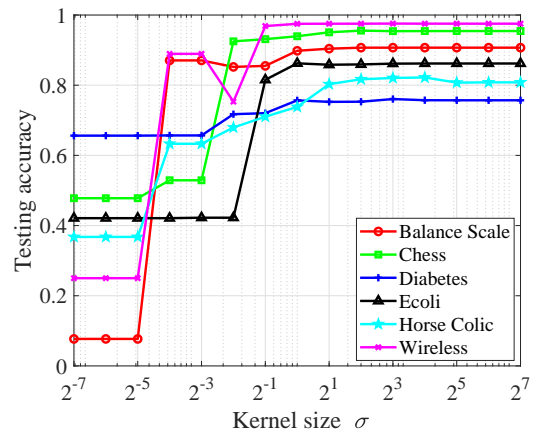
for C-BLS. Except for the grid search method adopted in this work, other productive technologies, like Silverman rule [30], [50], can also be good candidates to determine σ in practice.

B. Performance Evaluation of the Incremental Learning Algorithms

For large-scale datasets, there are usually a large number of samples and a high dimension. Once some new samples arrive or the network deems to be expanded, C-BLS needs to run a complete training cycle for remodeling the learning system, which not only results in large time consumption, but also requires large storage resources. As mentioned before, to guarantee that the system can be remodeled quickly without the entire retraining process from the beginning when some new samples arrive or the network deems to be expanded, we also develop several alternative incremental learning algorithms. In this part, we present experiments to demonstrate their effectiveness. Similar to [1], the Mixed National Institute of Standards and Technology (MNIST) handwriting dataset [51] which contains 60000 training samples and 10000 testing samples is adopted here for study purpose, and one can refer to [1], [51] for details about this dataset.



(a) Regression datasets



(b) Classification datasets

Fig. 4. The influence of kernel size σ on learning performance.

TABLE IV
RECOGNITION RESULTS ON MNIST DATASET AT DIFFERENT INCREMENTAL STEPS: INCREMENT OF TRAINING SAMPLES.

Training Samples	Training Time (s)	Testing Accuracy
20000	104.02 \pm 2.58	97.92 \pm 0.05
20000 \rightarrow 30000	50.58 \pm 1.77	98.12 \pm 0.04
30000 \rightarrow 40000	50.94 \pm 1.68	98.19 \pm 0.05
40000 \rightarrow 50000	51.17 \pm 2.27	98.26 \pm 0.04
50000 \rightarrow 60000	51.54 \pm 0.96	98.30 \pm 0.05

First, the receiving of new training samples is considered. Hence, we use the first 20000 samples to train the initial network, and then add 10000 additional samples to the network each time until all training samples are utilized. During the whole process, the N_f , N_m , N_e , γ and σ are respectively fixed at 10, 10, 5000, 10^{-5} and 2^5 , respectively. Table IV shows the training times and testing accuracies at different incremental steps when the network receives the new training samples. It can be seen from Table IV that, with the increment of the training samples, the testing accuracy increases as expected, and finally accuracy reaches at 98.30 ± 0.05 , which is comparable to the standard BLS when the same network allocation is

adopted (see Table V of Ref. [1] for details). Meanwhile, other than the initial stage, the subsequent incremental learning steps don't need to consume too much training time. This conforms the effective of the proposed incremental learning algorithms when some new training samples are received.

TABLE V
RECOGNITION RESULTS ON MNIST DATASET AT DIFFERENT INCREMENTAL STEPS: INCREMENTS OF FEATURE NODES AND ENHANCEMENT NODES.

(Feature Nodes, Enhancement Nodes)	Training Time (s)	Testing Accuracy
(10 × 6, 3000)	108.90 ± 1.60	97.96 ± 0.09
(10 × 6 → 10 × 7, 3000 → 3500)	15.02 ± 0.61	98.06 ± 0.14
(10 × 7 → 10 × 8, 3500 → 4000)	16.98 ± 0.51	98.16 ± 0.09
(10 × 8 → 10 × 9, 4000 → 4500)	22.36 ± 1.11	98.25 ± 0.09
(10 × 9 → 10 × 10, 4500 → 5000)	25.03 ± 0.99	98.29 ± 0.09

Then, the increments of feature nodes and enhancement nodes are considered. The training samples in this case are received in one time. For study purpose, we firstly train the initial network with 10 × 6 feature nodes and 3000 enhancement nodes. Subsequently, the additional feature nodes and enhancement nodes are added to the network for performance improvement. In detail, the number of additional feature nodes in each incremental step is fixed at 10 × 1, while the number of additional enhancement nodes in each incremental step is set as 500 (the first 200 correspond to the additional feature nodes, and the rest 300 are extra inserted). In Table V, we show the training times and testing accuracies at different incremental steps when both new feature nodes and enhancement nodes are inserted to network. It can be seen from Table V that, with the numbers of both feature nodes and enhancement nodes increase, the algorithm has the chance to get a higher recognition accuracy than the initial stage, while the training time in each incremental step don't need to be very high.

TABLE VI
RECOGNITION RESULTS ON MNIST DATASET AT DIFFERENT INCREMENTAL STEPS: INCREMENTS OF TRAINING SAMPLES AND ENHANCEMENT NODES.

(Training Samples, Enhancement Nodes)	Training Time(s)	Testing Accuracy
(20000, 1000)	8.44 ± 0.22	97.02 ± 0.12
(20000 → 30000, 1000 → 2000)	31.45 ± 0.97	97.66 ± 0.06
(30000 → 40000, 2000 → 3000)	42.35 ± 0.70	98.04 ± 0.06
(40000 → 50000, 3000 → 4000)	57.94 ± 1.52	98.08 ± 0.41
(50000 → 60000, 4000 → 5000)	78.87 ± 2.25	98.39 ± 0.07

Finally, the synchronous increments of training samples and enhancement nodes are considered. At the initial stage, only the first 20000 training samples are sent to network, while the number of enhancement nodes is set as 1000. At each subsequent incremental step, 10000 new training samples are sent to network and the additional number of enhancement nodes is set as 1000. Table VI shows the training times and testing accuracies at different incremental steps. As can be seen from Table VI, the proposed incremental learning algorithms can work well when both training samples and enhancement nodes increase.

C. Application to Time Series Prediction

In this subsection, the proposed C-BLS will be applied to perform time series prediction tasks. The presented examples include Mackey-Glass time series prediction and monthly mean total ‘‘Sunspot Number’’ prediction.

1) *Data sets*: Mackey-Glass time series displays the characteristics of chaotic dynamics, and can be described by the following time-delay differential equation:

$$\frac{dx(t)}{dt} = -bx(t) + \frac{ax(t - \tau)}{1 + x(t - \tau)} \quad (66)$$

where $a = 0.1$, $b = 0.2$ and $\tau = 30$ are the default choice in the current paper. Based on (66), we first generate 1200 data points, among which, the first 1000 are used for training and the rest 200 are used for testing. To comprehensively evaluate the performance of the proposed methods, the Gaussian signal sequence and the impulse signal sequence are respectively added to the training samples to model the influences caused by different disturbances. In detail, the Gaussian signal sequence is generated by a Gaussian distribution with zero-mean and variance of 0.01; the impulse signal sequence is generated by an α -stable distribution [22], [23] whose characteristic function can be simply formulated by $\psi(\omega) = \exp(-\gamma|\omega|^\alpha)$, where $\gamma = 0.1$ and $\alpha = 1.5$. As suggested in [23], we adopt the previous seven points to predict the current one. Hence, the input and output at time t have the form of $\mathbf{x}_t = [x(t-7), \dots, x(t-1)]$ and $y_t = x(t)$, respectively.

The ‘‘Sunspot Number’’ is a real time series dataset which records the number of monthly mean total sunspot from January 1749 to December 2017, and is available at <http://www.sidc.be/silso/datafiles>. In the following experiments, the data are firstly normalized into the range of [0, 1]. After that, the training set is constructed based on the sunspot number recorded from January 1749 to December 1990, while the testing set is constructed based on the sunspot number recorded from January 1991 to December 2017. Like [47], the embedding dimension and the delay time are respectively set as 4 and 1 in the experiments.

2) *Experimental Results*: When faced with time series prediction tasks, the standard BLS [5], the structured manifold BLS (SM-BLS) [7], the robust manifold BLS (RM-BLS) [19] and the recurrent BLS [10] have all been proven to be good candidates. Moreover, we note that the first three of them are developed based on the fully feedforward neural network model like the proposed C-BLS, so they are chosen as the benchmarks for comparison.

Table VII shows the main parameters setting and comparative results of different algorithms. It can be seen from Table VII that, if the noise sequence is drawn from Gaussian distribution, the standard BLS and SMBLS perform better than that of RMBLS and C-BLS. However, if the Gaussian assumption is not satisfied, their performance can be degenerated evidently. In contrary, the C-BLS can always obtain a relatively satisfactory prediction result in both Gaussian and alpha-stable noise environments. Moreover, the prediction results on real Sunspot number dataset also conform that C-BLS is a good candidate for time series prediction tasks.

TABLE VII
PERFORMANCE COMPARISON OF DIFFERENT METHODS ON TIME SERIES DATASETS.

Dataset	Algorithm	Parameters	Training Time (s)	Testing RMSE
Mackey-Glass (Gaussian)	BLS	$(N_f, N_w, N_e, \gamma) = (7, 13, 160, 10^{-5})$	0.0294 ± 0.0111	0.0483 ± 0.0042
	SM-BLS	$(N_f, N_w, N_e, \lambda, \alpha, \beta) = (15, 1, 180, 10^{-4}, 10^{-5}, 10^{-2})$	0.7158 ± 0.0158	0.0477 ± 0.0035
	RM-BLS	$(N_f, N_w, N_e, \lambda, \alpha, \beta) = (27, 1, 430, 10^{-2}, 10^0, 10^{-1})$	0.2902 ± 0.0071	0.0484 ± 0.0082
	C-BLS	$(N_f, N_w, N_e, \gamma, \sigma) = (7, 15, 160, 10^{-4}, 2^5)$	0.0487 ± 0.0030	0.0486 ± 0.0051
Mackey-Glass (α -stable)	BLS	$(N_f, N_w, N_e, \gamma) = (25, 17, 270, 10^{-4})$	0.0631 ± 0.0041	0.0909 ± 0.0123
	SM-BLS	$(N_f, N_w, N_e, \lambda, \alpha, \beta) = (29, 1, 420, 10^{-7}, 10^0, 10^{-2})$	1.0977 ± 0.0196	0.0921 ± 0.0030
	RM-BLS	$(N_f, N_w, N_e, \lambda, \alpha, \beta) = (27, 1, 360, 10^{-7}, 10^{-1}, 10^{-2})$	0.2834 ± 0.0053	0.0873 ± 0.0045
	C-BLS	$(N_f, N_w, N_e, \gamma, \sigma) = (25, 20, 456, 10^{-4}, 2^{-2})$	1.6315 ± 0.0283	0.0547 ± 0.0035
Sunspot Number	BLS	$(N_f, N_w, N_e, \gamma) = (25, 13, 150, 10^{-3})$	0.0697 ± 0.0019	0.0543 ± 0.0013
	SM-BLS	$(N_f, N_w, N_e, \lambda, \alpha, \beta) = (23, 1, 50, 10^{-5}, 10^{-2}, 10^{-2})$	6.0065 ± 0.1869	0.0536 ± 0.0004
	RM-BLS	$(N_f, N_w, N_e, \lambda, \alpha, \beta) = (7, 1, 90, 10^{-2}, 10^{-1}, 10^{-3})$	1.3597 ± 0.0118	0.0531 ± 0.0006
	C-BLS	$(N_f, N_w, N_e, \gamma, \sigma) = (29, 13, 30, 10^{-2}, 2^{-3})$	0.4470 ± 0.0913	0.0530 ± 0.0003

D. Application to EEG Classification

Electroencephalography (EEG) is a kind of neurophysiological signal, which is generated by the firing of neurons in the brain and usually collected via electrodes placed on the scalp surface (see Fig. 5 for a glimpse). Due to its safety, inexpensiveness, non-invasiveness and a favorable temporal resolution (on the precision of milliseconds), EEG has been becoming an indispensable role in the applications of Brain-Compute-Interface (BCI) [52]. During the past few years, many efforts have been devoted to improving the EEG classification accuracy of the EEG-based BCI systems. However, because of the inherent complexity of EEG signals (such as high dimensionality, high dynamic and low signal-noise-ratio (SNR)), the corresponding classification result, up to today, still cannot meet the application requirements. In this subsection, we will try to apply the proposed C-BLS to EEG classification tasks.

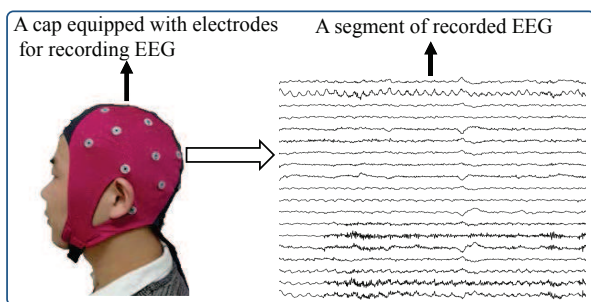


Fig. 5. A glimpse of recording EEG.

1) *Data sets*: The benchmark dataset adopted here is the data set 2b of BCI competition IV [53], which includes the EEG recordings from nine healthy subjects. For each subject, there are five sessions about two-classes motor imagery tasks (left hand VS right hand). Among the five sessions, the first two of them were recorded without feedback and each of them includes 120 trials, while the other three sessions were incorporated with online feedback and each of them has 160 trials. In each session, three channels including C3, Cz and C4 were used to record EEG measurements with a sampling

frequency of 250 HZ. To remove the influence caused by the power equipments, the EEG sequences had been bandpass filtered from 0.5 HZ to 100 HZ and a notch filter at the notch frequency of 50 HZ had also been adopted. In the following experiments, the EEG recordings from the first three sessions are used for training and the EEG recordings from the last two sessions are used for testing.

2) *Reprocessing and Feature Extraction*: In order to exclude the EEG recordings that are not related to motor imagery tasks, only the segment between 0.5 s and 2.5 s after cue is kept in each trial. These reserved EEG segments are subsequently bandpass filtered from 8 HZ to 35 HZ as recommended in [53]. Moreover, since the brain activities reflecting the imaginary limb motion mainly exist in the contralateral region of the brain, the data from channel Cz is removed in our experiments. Without loss of generality, the MATLAB command “pwelch”, with a sliding Hamming window of 0.25 s and an overlap of 0.125 s, is used for computing the power spectrum density (PSD) [54], [55] of the EEG data in C3 and C4. Similar to [55], the number of discrete-Fourier-transform (DFT) points is set as 256, and the final feature vector for each trail is obtained by concatenating the PSD values of C3 and C4 channels.

3) *Parameters Setting and Results*: Other than the standard BLS, several classical classifiers, including K-nearest neighbors (K-NN) [56], support vector machine (SVM) [57], extreme learning machine (ELM) [58], DBN [3] and SAE [4], are also chosen as the benchmark for comparison. The parameter search ranges of different algorithms are as follows.

- For BLS and C-BLS, the regularization parameter in them are both chosen from the range of $\{10^{-5}, 10^{-4}, \dots, 10^4, 10^5\}$, while the remainder parameter are searched within the ranges detailed in Section IV-A.
- For K-NN, we choose the number of k from 1 to 10 with the step-size of 1.
- For SVM, the Gaussian kernel is adopted. After that, the kernel size and regularization parameter are searched from $\{2^{-5}, 2^{-4}, \dots, 2^4, 2^5\}$ and $\{10^{-5}, 10^{-4}, \dots, 10^4, 10^5\}$, respectively.

- For ELM, the sigmoid activation function is adopted with the input weights and biases randomly generated from $[-1, 1]$ and $[0, 1]$, respectively. Meanwhile, we perform a grid search for its number of hidden nodes from $[5 : 600]$ with the step size of 5 and regularization parameter from $\{10^{-5}, 10^{-4}, \dots, 10^4, 10^5\}$.
- For DBN and SAE, they are implemented using “DeepLearnToolbox” [59]. Herein, only two hidden-layers are involved, and the optimal number of neurons at the first and the second layer are both chosen from $[20 : 300]$ with the step-size of 20. In addition, the number of epoches for unsupervised and supervised learning stages are respectively set as 150 and 100, the learning rates for unsupervised and supervised learning stages are respectively set as 1.5 and 1.0, the mini-batch sizes for supervised and unsupervised learning stages are both fixed at 20, and the activation function in the network is set as the sigmoid function.

TABLE VIII
TESTING ACCURACIES OF DIFFERENT CLASSIFIERS ON DATA SET IIB OF
BCI COMPETITION IV (IN %)

Subject	Classifier						
	K-NN	SVM	ELM	SAE	DBN	BLS	C-BLS
B01	60.31	69.69	67.34	67.69	65.44	71.03	71.22
B02	56.43	61.79	59.57	57.18	54.82	60.21	61.89
B03	53.44	54.38	53.47	52.84	52.37	52.97	52.97
B04	96.56	95.31	95.91	95.56	93.09	93.91	93.50
B05	70.94	87.81	87.28	86.59	83.88	86.34	87.25
B06	75.00	78.44	79.66	78.59	71.31	79.97	82.22
B07	67.81	64.69	70.50	70.63	63.88	71.81	71.97
B08	88.44	90.00	91.25	90.22	85.03	90.28	91.59
B09	78.75	80.31	80.12	79.78	79.09	80.38	80.59
Mean	71.96	75.82	76.12	75.45	72.10	76.32	77.02

Table VIII shows the classification results of different methods. It can be seen from Table VIII that, C-BLS can obtain a higher testing classification accuracy on most subjects and it also has the highest average classification accuracy on all subjects. These results suggest that the proposed C-BLS can be, at least, a better candidate compared with the standard BLS and several other classical classifiers when applied to EEG classification tasks.

V. CONCLUSION

To enhance the robustness of Broad Learning System (BLS), the maximum correntropy criterion (MCC) was introduced to train its output weights, generating a correntropy based BLS (C-BLS). To ensure that the system can be updated quickly without the entire retraining process from the beginning when some new samples arrive or the network deems to be expanded, three alternative incremental learning algorithms were then developed. As we know, this is the first attempt to combine the Information Theoretic Learning (ITL) criterion and the BLS architecture. Experimental results showed that the proposed C-BLS is not only robust to outliers but also can be a good candidate if we don't know any prior information about

the noise distribution in some practical scenarios. Meanwhile, the proposed incremental learning algorithms were proven to have the ability to support rapid remodeling. In the future, the flexibly combinations of C-BLS with some well-developed feature mapping technologies, like convolution-pooling operation [5], neuro-fuzzy model [6], and structured manifold learning method [7], will be considered for further performance improvement.

REFERENCES

- [1] C. L. P. Chen and Z. Liu, “Broad learning system: An effective and efficient incremental learning system without the need for deep architecture,” *IEEE Trans. Neural Netw. Learn. Syst.*, vol. 29, no. 1, pp. 10–24, Jan. 2018.
- [2] C. M. Bishop, *Pattern recognition and machine learning*. New York, NY, USA: Springer-Verlag, 2006.
- [3] S. O. Geoffrey E. Hinton and Y. W. Teh, “A fast learning algorithm for deep belief nets,” *Neural Comput.*, vol. 18, no. 7, pp. 1527–1554, Jul. 2006.
- [4] P. Vincent, H. Larochelle, I. Lajoie, Y. Bengio, and P.-A. Manzagol, “Stacked denoising autoencoders: Learning useful representations in a deep network with a local denoising criterion,” *J. Mach. Learn. Res.*, vol. 11, pp. 3371–3408, Dec. 2010.
- [5] C. L. P. Chen, Z. Liu, and S. Feng, “Universal approximation capability of broad learning system and its structural variations,” *IEEE Trans. Neural Netw. Learn. Syst.*, pp. 1–14, 2018.
- [6] S. Feng and C. L. P. Chen, “Fuzzy broad learning system: A novel neuro-fuzzy model for regression and classification,” *IEEE Trans. Cybern.*, pp. 1–11, 2018.
- [7] M. Han, S. Feng, C. L. P. Chen, M. Xu, and T. Qiu, “Structured manifold broad learning system: A manifold perspective for large-scale chaotic time series analysis and prediction,” *IEEE Trans. Knowl. Data Eng.*, vol. 31, no. 9, pp. 1809–1821, Sept. 2019.
- [8] J. Jin, Z. Liu, and C. L. P. Chen, “Discriminative graph regularized broad learning system for image recognition,” *Sci. China-Inf. Sci.*, vol. 61, no. 11, p. 112209, Oct. 2018.
- [9] J. Jin and C. L. P. Chen, “Regularized robust broad learning system for uncertain data modeling,” *Neurocomputing*, vol. 322, pp. 58 – 69, 2018.
- [10] M. Xu, M. Han, C. L. P. Chen, and T. Qiu, “Recurrent broad learning systems for time series prediction,” *IEEE Trans. Cybern.*, pp. 1–13, 2018.
- [11] Y. Kong, X. Wang, Y. Cheng, and C. L. P. Chen, “Hyperspectral imagery classification based on semi-supervised broad learning system,” *Remote Sens.*, vol. 10, no. 5, p. 585, 2018.
- [12] T. Zhang, R. Chen, X. Yang, and S. Guo, “Rich feature combination for cost-based broad learning system,” *IEEE Access*, vol. 7, pp. 160–172, 2019.
- [13] Q. Zhou and X. He, “Broad learning model based on enhanced features learning,” *IEEE Access*, vol. 7, pp. 42536–42550, 2019.
- [14] J. Zou, Q. She, F. Gao, and M. Meng, “Multi-task motor imagery EEG classification using broad learning and common spatial pattern,” in *2018 International Conference on Intelligence Science*, 2018, pp. 3–10.
- [15] H. Guo, B. Sheng, P. Li, and C. L. P. Chen, “Multiview high dynamic range image synthesis using fuzzy broad learning system,” *IEEE Trans. Cybern.*, pp. 1–13, 2019.
- [16] J. Han, L. Xie, J. Liu, and X. Li, “Personalized broad learning system for facial expression,” *Multimed. Tools Appl.*, Jul 2019. [Online]. Available: <https://doi.org/10.1007/s11042-019-07979-2>
- [17] W. Yu and C. Zhao, “Broad convolutional neural network based industrial process fault diagnosis with incremental learning capability,” *IEEE Trans. Ind. Electron.*, pp. 1–1, 2019.
- [18] F. Chu, T. Liang, C. L. P. Chen, X. Wang, and X. Ma, “Weighted broad learning system and its application in nonlinear industrial process modeling,” *IEEE Trans. Neural Netw. Learn. Syst.*, pp. 1–15, 2019.
- [19] S. Feng, W. Ren, M. Han, and Y. W. Chen, “Robust manifold broad learning system for large-scale noisy chaotic time series prediction: A perturbation perspective,” *Neural Netw.*, vol. 117, pp. 179–190, 2019.
- [20] M. Li and D. Wang, “Insights into randomized algorithms for neural networks: Practical issues and common pitfalls,” *Inf. Sci.*, vol. 382–383, pp. 170 – 178, 2017.
- [21] J. C. Principe, *Information Theoretic Learning: Renyi's Entropy and Kernel Perspectives*. New York, NY, USA: Springer, 2010.

- [22] Z. Wu, J. Shi, X. Zhang, W. Ma, and B. Chen, "Kernel recursive maximum correntropy," *Signal Process.*, vol. 117, pp. 11–16, Dec. 2015.
- [23] S. Wang, Y. Zheng, S. Duan, L. Wang, and H. Tan, "Quantized kernel maximum correntropy and its mean square convergence analysis," *Digit. Signal Process.*, vol. 63, pp. 164–176, Apr. 2017.
- [24] B. Chen, X. Liu, H. Zhao, and J. C. Príncipe, "Maximum correntropy kalman filter," *Automatica*, vol. 76, pp. 70–77, 2017.
- [25] M. Li, C. Huang, and D. Wang, "Robust stochastic configuration networks with maximum correntropy criterion for uncertain data regression," *Inf. Sci.*, vol. 473, pp. 73–86, 2019.
- [26] Y. Guo, F. Wang, B. Chen, and J. Xin, "Robust echo state networks based on correntropy induced loss function," *Neurocomputing*, vol. 267, pp. 295–303, 2017.
- [27] X. Luo, Y. Xu, W. Wang, M. Yuan, X. Ban, Y. Zhu, and W. Zhao, "Towards enhancing stacked extreme learning machine with sparse autoencoder by correntropy," *J. Frankl. Inst.*, vol. 355, no. 4, pp. 1945–1966, 2018.
- [28] L. Chen, H. Paul, H. Qu, J. Zhao, and X. Sun, "Correntropy-based robust multilayer extreme learning machines," *Pattern Recognit.*, vol. 84, pp. 357–370, 2018.
- [29] H. Xing and X. Wang, "Training extreme learning machine via regularized correntropy criterion," *Neural Comput. Appl.*, vol. 23, no. 7, pp. 1977–1986, Dec. 2013.
- [30] R. He, B. Hu, W. Zheng, and X. Kong, "Robust principal component analysis based on maximum correntropy criterion," *IEEE Trans. Image Process.*, vol. 20, no. 6, pp. 1485–1494, Jun. 2011.
- [31] Y. Qi, Y. Wang, X. Zheng, and Z. Wu, "Robust feature learning by stacked autoencoder with maximum correntropy criterion," in *2014 IEEE International Conference on Acoustics, Speech and Signal Processing (ICASSP)*, May 2014, pp. 6716–6720.
- [32] L. Chen, H. Qu, J. Zhao, B. Chen, and J. C. Príncipe, "Efficient and robust deep learning with correntropy-induced loss function," *Neural Comput. Appl.*, vol. 27, no. 4, pp. 1019–1031, 2016.
- [33] J. Dong, B. Chen, N. Lu, H. Wang, and N. Zheng, "Correntropy induced metric based common spatial patterns," in *2017 IEEE 27th International Workshop on Machine Learning for Signal Processing (MLSP)*, Sept. 2017, pp. 1–6.
- [34] W. Liu, P. P. Pokharel, and J. C. Príncipe, "Correntropy: properties and applications in non-Gaussian signal processing," *IEEE Trans. Signal Process.*, vol. 55, no. 11, pp. 5286–5298, Nov. 2007.
- [35] Y. H. Pao, G. H. Park, and D. J. Sobajic, "Learning and generalization characteristics of the random vector functional-link net," *Neurocomputing*, vol. 6, no. 2, pp. 163–180, Apr. 1994.
- [36] C. L. P. Chen and J. Z. Wan, "A rapid learning and dynamic stepwise updating algorithm for flat neural networks and the application to time-series prediction," *IEEE Trans. Syst. Man Cybern.*, vol. 29, no. 1, pp. 62–72, Feb. 1999.
- [37] N. Aronszajn, "Theory of reproducing kernels," *Trans. Amer. Math. Soc.*, vol. 68, no. 3, pp. 337–404, May 1950.
- [38] B. Chen, L. Xing, H. Zhao, S. Du, and J. C. Príncipe, "Effects of outliers on the maximum correntropy estimation: A robustness analysis," *IEEE Trans. Syst. Man Cybern. -Syst.*, pp. 1–6, 2019.
- [39] L. Bako, "Robustness analysis of a maximum correntropy framework for linear regression," *Automatica*, vol. 87, pp. 218–225, 2018.
- [40] F. Zhu, A. Halimi, P. Honeine, B. Chen, and N. Zheng, "Correntropy maximization via ADMM: Application to robust hyperspectral unmixing," *IEEE Trans. Geosci. Remote Sensing*, vol. 55, no. 9, pp. 4944–4955, Sept. 2017.
- [41] R. He, W. Zheng, and B. Hu, "Maximum correntropy criterion for robust face recognition," *IEEE Trans. Pattern Anal. Mach. Intell.*, vol. 33, no. 8, pp. 1561–1576, Aug. 2011.
- [42] Y. Feng, X. Huang, S. Lei, Y. Yang, and J. A. K. Suykens, "Learning with the maximum correntropy criterion induced losses for regression," *J. Mach. Learn. Res.*, vol. 16, no. 1, pp. 993–1034, 2015.
- [43] R. P. Agarwal, M. Meehan, and D. O'Regan, *Fixed Point Theory and Applications*. Cambridge, U.K.: Cambridge University Press, 2001.
- [44] B. Chen, J. Wang, H. Zhao, N. Zheng, and J. C. Príncipe, "Convergence of a fixed-point algorithm under maximum correntropy criterion," *IEEE Signal Process. Lett.*, vol. 22, no. 10, pp. 1723–1727, Oct. 2015.
- [45] A. R. Heravi and G. A. Hodtani, "A new robust fixed-point algorithm and its convergence analysis," *J. Fixed Point Theory Appl.*, vol. 19, no. 4, pp. 3191–3215, Dec. 2017.
- [46] B. Chen, L. Xing, X. Wang, J. Qin, and N. Zheng, "Robust learning with kernel mean p -power error loss," *IEEE Trans. Cybern.*, vol. 48, no. 7, pp. 2101–2113, Jul. 2018.
- [47] W. Liu, J. C. Príncipe, and S. Haykin, *Kernel adaptive filtering : a comprehensive introduction*. New York: Wiley, 2010.
- [48] D. Dua and C. Graff, "UCI machine learning repository," 2017. [Online]. Available: <http://archive.ics.uci.edu/ml>
- [49] S. V. Huffel, "Partial singular value decomposition algorithm," *J. Comput. Appl. Math.*, vol. 33, no. 1, pp. 105–112, 1990.
- [50] B. W. Silverman, *Density Estimation for Statistics and Data Analysis*. London, U.K.: Chapman and Hall, 1986, vol. 3.4.2.
- [51] Y. Lecun, L. Bottou, Y. Bengio, and P. Haffner, "Gradient-based learning applied to document recognition," *Proceedings of the IEEE*, vol. 86, no. 11, pp. 2278–2324, 1998.
- [52] A. E. Hassanien and A. A. Azar, *Brain-Computer Interfaces*. Switzerland: Springer, 2015.
- [53] R. Leeb, F. Lee, C. Keinrath, R. Scherer, H. Bischof, and G. Pfurtscheller, "Brain-computer communication: Motivation, aim, and impact of exploring a virtual apartment," *IEEE Trans. Neural Syst. Rehabil. Eng.*, vol. 15, no. 4, pp. 473–82, 2007.
- [54] P. Welch, "The use of fast Fourier transform for the estimation of power spectra: a method based on time averaging over short, modified periodograms," *IEEE Transactions on audio and electroacoustics*, vol. 15, no. 2, pp. 70–73, 1967.
- [55] K. P. Thomas and A. P. Vinod, "EEG-based biometric authentication using gamma band power during rest state," *Circuits Syst. Signal Process.*, vol. 37, no. 1, pp. 277–289, 2018.
- [56] J. M. Keller, M. R. Gray, and J. A. Givens, "A fuzzy k-nearest neighbor algorithm," *IEEE Trans. Syst. Man Cybern.*, vol. 15, no. 4, pp. 580–585, Jul. 1985.
- [57] C. Cortes and V. Vapnik, "Support-vector networks," *Mach. Learn.*, vol. 20, no. 3, pp. 273–297, Sept. 1995.
- [58] G. Huang, Q. Zhu, and C. K. Siew, "Extreme learning machine: Theory and applications," *Neurocomputing*, vol. 70, no. 1, pp. 489–501, 2006.
- [59] R. B. Palm, "Prediction as a candidate for learning deep hierarchical models of data," Master's thesis, Technical University of Denmark, 2012.